ACS chemical biology

Articles

pubs.acs.org/acschemicalbiology

The Dynamics Behind the Affinity: Controlling Heme-Gas Affinity *via* Geminate Recombination and Heme Propionate Conformation in the NO Carrier Cytochrome *c′*

Colin R. Andrew,[†] Olga N. Petrova,[‡] Isabelle Lamarre,[‡] Jean-Christophe Lambry,[‡] Fabrice Rappaport,[§] and Michel Negrerie*[,‡]

[†]Department of Chemistry and Biochemistry, Eastern Oregon University, La Grande, Oregon 97850, United States

[‡]Laboratoire d'Optique et Biosciences, INSERM, Ecole Polytechnique, 91128 Palaiseau, France

[§]Laboratoire de Physiologie Membranaire et Moléculaire du Chloroplaste, CNRS, Université Pierre et Marie Curie, 75005 Paris, France

Supporting Information

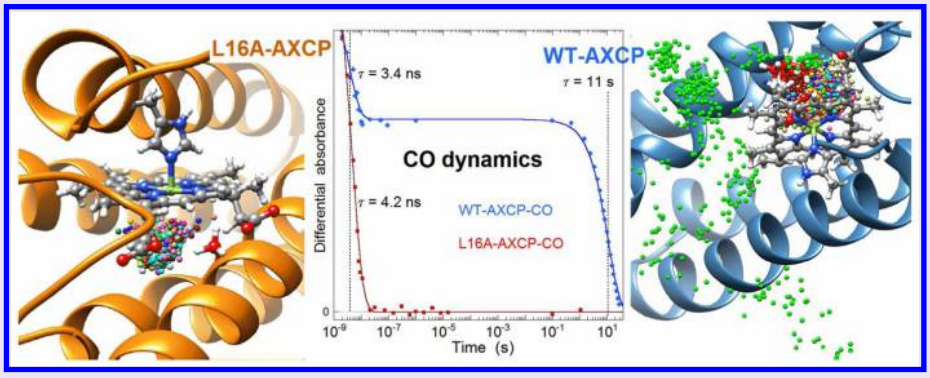

ABSTRACT: Nitric oxide (NO) sensors are heme proteins which may also bind CO and O_2. Control of heme-gas affinity and their discrimination are achieved by the structural properties and reactivity of the heme and its distal and proximal environments, leading to several energy barriers. In the bacterial NO sensor cytochrome *c′* from *Alcaligenes xylosoxidans* (AXCP), the single Leu16Ala distal mutation boosts the affinity for gas ligands by a remarkable 10^6−10^8-fold, transforming AXCP from one of the lowest affinity gas binding proteins to one of the highest. Here, we report the dynamics of diatomics after photodissociation from wild type and L16A-AXCP over 12 orders of magnitude in time. For the L16A variant, the picosecond geminate rebinding of both CO and NO appears with an unprecedented 100% yield, and no exit of these ligands from protein to solvent could be observed. Molecular dynamic simulations saliently demonstrate that dissociated CO stays within 4 Å from Fe^{2+}, in contrast to wild-type AXCP. The L16A mutation confers a heme propionate conformation and docking site which traps the diatomics, maximizing the probability of recombination and directly explaining the ultrahigh affinities for CO, NO, and O_2. Overall, our results point to a novel mechanism for modulating heme-gas affinities in proteins.

It is established that the affinity of a ligand for a protein is controlled by energy barriers that may originate either from the protein structure or from the enthalpy of interaction and may be multiple within the same protein. The modulation of these energy barriers allows the precise adjustment of the kinetic rate constants for ligand binding (k_{on}) and release (k_{off}) and consequently of the affinity by evolutive mutations. Gas-binding heme proteins, whatever their function, require a precise discrimination between XO species (X = N, O, C). For heme proteins that form six-coordinate Fe^{2+}(XO) gas complexes with a proximal His ligand, the relative binding affinities of diatomics have been rationalized by the "sliding scale" rule.[1] The increase or decrease of one energy barrier (for example, steric hindrance for entry into the heme pocket) acting in the same manner for all three diatomic ligands leads to a proportional change of the rates, seen as an overall "slide" of their log-pattern.[1]

The first mechanism of discrimination between NO and CO binding is the enthalpic barrier: the electronic properties of NO enable it to bind to Fe^{2+} even if it is located out of the heme plane (domed heme), contrary to CO, whose binding requires iron fluctuations toward the heme plane.[2−5] This enthalpic barrier, which does not exist for NO, increases the probability of CO escape from domed hemes. Differential ability for back bonding between the ligands and the iron orbitals also influences the association rates.[6] The sliding scale reflects

Received: July 12, 2016
Accepted: October 6, 2016
Published: October 6, 2016

DOI: 10.1021/acschembio.6b00599
ACS Chem. Biol. 2016, 11, 3191−3201

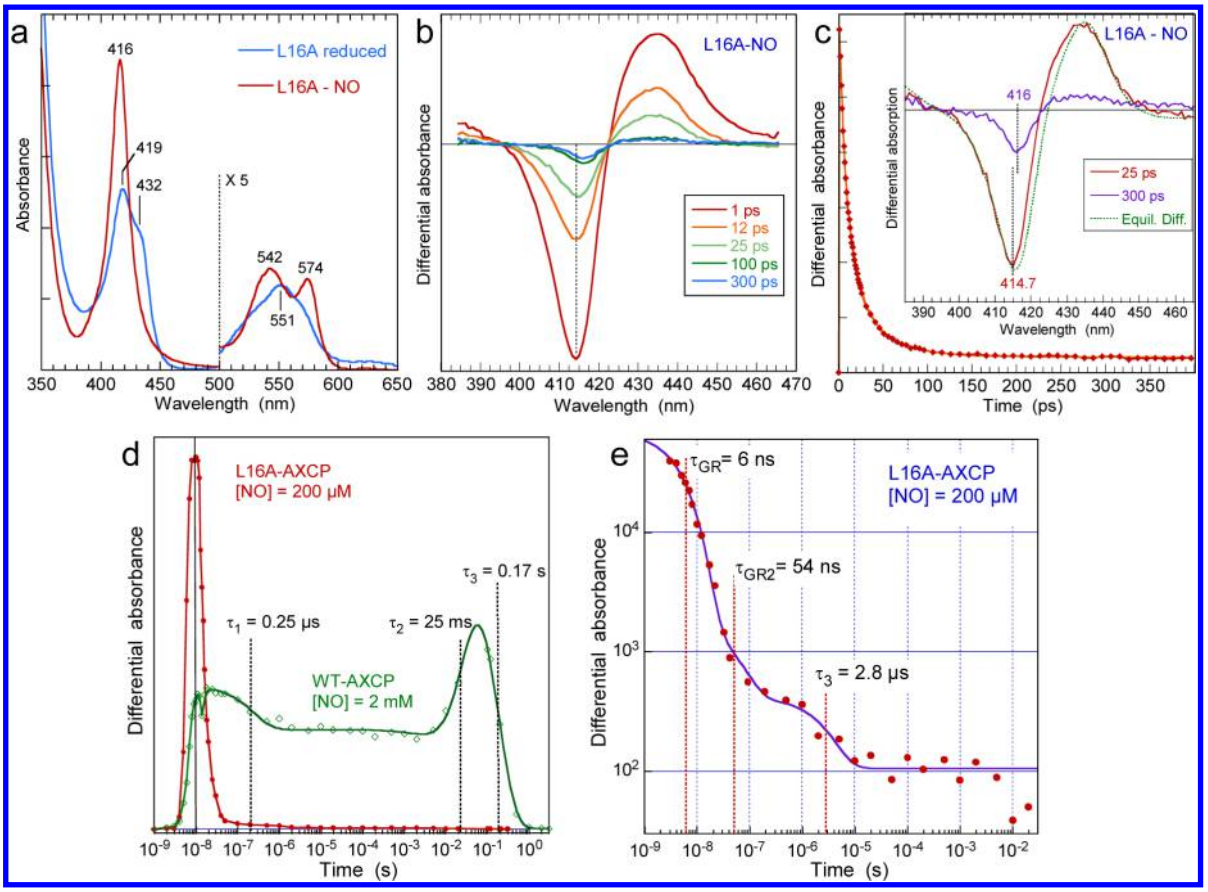

Figure 1. Kinetics of NO rebinding to L16A-AXCP from 1 ps to 1 s. (a) Equilibirum spectra of ferrous L16A-AXCP unliganded and NO-liganded. (b) Transient absorption spectra at selected time delays after NO photodissociation recorded with a 50 fs probe pulse. (c) Kinetics of NO rebinding to the heme in the ps time range. Inset: comparison of the difference transient spectra at 25 and 300 ps with the steady-state difference spectrum (green dotted line). (d) The kinetics of NO rebinding to L16A-AXCP, probed at 432 nm in the nanosecond to second time range, are compared to those of WT-AXCP measured at 418 nm and fitted to a multiexponential function. (e) Double-log view of the L16A-AXCP kinetics fitted in the entire time range together with the time constants. The time origin in panel *d* is that of the electronic delay, whereas the time origin for fitting the data points in panel *e* was set to the maximum of the initial absorption rise. The NO concentration was 200 μM for L16A-AXCP and 2 mM for WT-AXCP. T = 20 °C.

these electronic discriminations and is also modulated by steric barrier(s) from the protein structure which most often influences all three diatomics in the same manner. In addition to this enthalpic barrier, other factors may exist influencing the dynamics of the gaseous ligands, and thus their discrimination. These effects have been probed extensively in myoglobin[1,7−10] and peroxidases,[11,12] and recent studies have also investigated ligand discrimination in heme sensors of the H-NOX (heme nitric oxide/oxygen binding)[13] and cytochrome *c*′ families.[14]

Among heme sensors, cytochromes *c*′ (Cyt *c*′) are found in denitrifying, nitrogen-fixing, methanotrophic, and some other bacteria. They structurally differ from the mitochondrial cytochrome *c*, sharing only the attachment of the heme to the protein by covalent links with sulfur atoms from cysteines (*c*-type heme). Previous studies attempted to decipher the role of Cyt *c*′ and reported its reaction with NO in correlation with bacteria living conditions.[15−18] In particular, Cyt *c*′ from *Rhodobacter capsulatus* confers a higher resistance to NO present in the bacteria growth medium[15] and has a role in NO removal, maybe coupled to reductase activity.[16] On the other hand, Cyt *c*′ is more highly expressed in denitrifying conditions in *Rhodobacter sphaeroides*, without reductase activity,[17] suggesting a role as a NO transporter.[17,18] Thus, the exact biochemical function of Cyt *c*′ is not resolved, but the hypothesis of a role as NO sensor or transporter[17,18] is supported by the formation of the 5c-NO species and the "one-way-gate" mechanism of NO release.[19,20] A more complete picture of its putative role can be found in ref 14.

In Cyt *c*′ from the bacterium *Alcaligenes xylosoxidans* (AXCP), the distal heme pocket is buried inside the protein and possesses hydrophobic residues which creates steric restrictions to the binding of gaseous ligands. Contrastingly, the proximal heme pocket is exposed to the solvent. The sterically hindered distal site results in low CO affinity (K_D ~ 0.28 mM) and no observable O_2 complex. In the absence of diatomics, the Fe(II) heme is 5-coordinate (5c), having a bond with the proximal His as the axial ligand, but in the presence of NO, the Fe(II) heme first forms a 6c-NO precursor in which the bound distal NO induces the rupture of the proximal Fe-His bond, yielding a distal 5c-NO complex. Then, a second NO replaces the His and the heme forms finally an unusual proximal 5c-NO complex *via* a putative unstable dinitrosyl species.[21,22] On the contrary, AXCP forms with CO the "classical" 6c-CO complex with no displacement of the proximal His. The reactivity with NO resembles that of the mammalian NO-receptor soluble guanylate cyclase (sGC) and other members of the H-NOX family[23−25] whose structure is very different from that of AXCP, which has a four helix bundle

DOI: 10.1021/acschembio.6b00599
ACS Chem. Biol. 2016, 11, 3191−3201

and two covalent thioester links which tightly maintain the heme.

Remarkably, the single mutation L16A in the distal heme pocket transforms the AXCP heme reactivity. In the mutant L16A-AXCP, NO forms a stable 6c-NO species without rupture of the Fe-His bond[26] so that the NO reactivity is solely determined by the heme distal side. The affinity of distal NO and CO increase by factors of 10^6 and 10^8, respectively ($K_{D(NO)} \sim 70$ fM, $K_{D(CO)} \sim 3$ pM).[26,27] Furthermore, wild type AXCP does not bind O_2, whereas the L16A-AXCP mutant does bind O_2 with a K_D of 49 nM,[26] which represents an 18-fold larger affinity with respect to myoglobin. According to the "sliding scale" rule,[1] one can estimate the K_D of $O_2 \geq 10^{-2}$ M for WT-AXCP (to be compared with the O_2 concentration of $\sim 10^{-3}$ M for an aqueous phase in equilibrium with the atmosphere), implying a theoretical increase of affinity of $\geq 2 \times 10^5$ induced by the L16A mutation.

Here, we aimed at understanding the origin of the very high affinity and demonstrating that the discrimination between the three diatomic ligands CO, NO, and O_2 can be governed by constraints at the heme level which can supplant other factors (such as steric hindrances in the access channel, reactivity of the ligand XO with the ferrous heme, and ligand stabilization by hydrogen bonds pattern). We measured the dynamics of these diatomics over 12 orders of magnitude in time after their photodissociation from the ferrous heme of the L16A mutant of AXCP. This broad time range allowed us to probe both the dynamics of geminate rebinding (the very same molecule which was photodissociated) and bimolecular rebinding (any molecule diffusing from the solvent) to the heme iron. These dynamics, governed by both internal energy barriers and heme reactivity, directly determine the affinity of the ligands. The data reveal that in the case of CO and NO, whose affinities for L16A-AXCP are the largest ever measured, the bimolecular rebinding is absolutely not detectable (its amplitude is close to zero) because these dissociated ligands are trapped very closely to the heme iron, so that the probability of geminate rebinding is maximized.

RESULTS AND DISCUSSION

Dynamics of Nitric Oxide. The Soret band of the reduced L16A-AXCP variant displays a doublet with a maximum at 418.5 nm and a shoulder at 432 nm (Figure 1a). This differs slightly from ferrous wt AXCP, which has a maximum at ∼424 nm and a shoulder at ∼434 nm.[14] Whereas resonance Raman spectra of ferrous wt AXCP assign both doublet features to a single 5c-HS heme chromophore,[28] there is evidence that ferrous L16A contains a minor population of 6c-LS species due to a small fraction of sites with distal heme ligation.[26] The external ligand could be either H_2O (unusual for a ferrous heme), O_2, or residual CO which is partly bound to the as-isolated L16A protein.[27] Thourough degassing of the sample and use of reductant should have removed any possible residual liganded O_2 ($k_{off} = 0.17$ s^{-1}).[26] In the presence of NO, the Soret maximum shifts to 416 nm as a sharp band. After photodissociation of NO, the corresponding bleaching band appears (415 nm) with the induced absorption counterpart at 434 nm (Figure 1b and c). Their amplitude rapidly decreased up to 300 ps, but with a slight shift of the bleaching from 414.5 to 416 nm (inset in Figure 1c). This later minor component cannot be due to a possible small amount of remaining O_2 because of two strong arguments which favor its assignment to NO. First, the photodissociated O_2 experiences diffusion to the solvent, even if diffusion represents a small amplitude compared to geminate O_2 rebinding. Because the concentration of O_2 is zero in the solution due to thourough degassing and to the large concentration of the reductant, O_2 has an almost null probability of bimolecular rebinding, so that this component should not be observed. Second, we measured a constant induced signal from ∼100 to 400 ps (Figure 1c), which is not the behavior of O_2, as described below. Consequently, these kinetics are only assigned to NO. They were fitted to the sum of two exponential functions, yielding the time constants τ_{G1} = 13.9 ps (A_{G1} = 67.3%) and τ_{G2} = 41 ps (A_{G2} = 26.7%) and a constant term (A_3 = 6%) which represents all other slower components (Table 1). The presence of two geminate rebinding components is a common property of 6-coordinate NO heme proteins.[5,29] Specifically, the fast component, which corresponds to NO still located in the heme pocket, has the same time constant as in myoglobin (14 ps). The second geminate component corresponds to NO escaped from the heme pocket but still present in the protein core, whereas the constant A_3 corresponds to NO diffusing farther than the heme pocket. This behavior agrees with the evolution of the transient IR spectra over 1 ns.[30]

Table 1. Kinetics of NO Geminate Rebinding to the Mutant L16A-AXCP, Compared with Other 6c-NO Heme Proteins and 5c-NO WT-AXCP

		NO geminate rebinding			bimolecular rebinding
protein[a]	ref	τ_1 (A_1)[b]	τ_2 (A_2)	τ_3 (A_3); τ_4 (A_4)	A_4 (%)
L16A-AXCP	this work	13.9 ps (67.3)	41 ps (26.7)	6 ns (6), 54 ns (<0.2)	0
WT AXCP 6c-NO (distal)	20		52 ps (43)		ND
WT AXCP 5c-NO (proximal)	20, 55	7 ps (98)			2
sGC	49	7.5 ps (97)			3
WT Mb	5	13 ps (40)	148 ps (50)		10
Lp-HbI	29	8.0 ps (36)	90 ps (62)		2
Ferric eNOS	49	15 ps (7)	200 ps (30)	2 ns (53)	10

[a]Abbreviations: Mb, myoglobin; eNOS, endothelial NO-synthase; *Lp*-Hb, hemoglobin from *Lucina Pectinata*; ND, not determined. [b]A_i (%) are the relative amplitudes of each exponential component.

This constant component was further investigated by recording the dynamics of NO rebinding up to 0.3 s (Figure 1d) by means of a detection system[31] whose sensitivity allows the measurements of variation as low as $\Delta OD/OD = 10^{-5}$. We probed the disappearance of the unliganded heme at 432 nm. Fitting the kinetics over the entire time range results in three time constants, τ_3 = 6 ns, τ_4 = 54 ns, and τ_5 = 2.8 μs, but no other components at larger time delays (Figure 1e). First, we must note that the duration of the photodissociating pulse of 5 ns is much longer than the geminate rebinding whose yield is high (φ_G = 94%). This implies that over 5 ns the same molecule L16A-AXCP-NO has the ability to dissociate and reform several times, inducing an apparent larger photodissociation yield, but the picosecond geminate rebinding remains the major process. The total amplitude of all components in the nanosecond to millisecond time range

DOI: 10.1021/acschembio.6b00599
ACS Chem. Biol. 2016, 11, 3191−3201

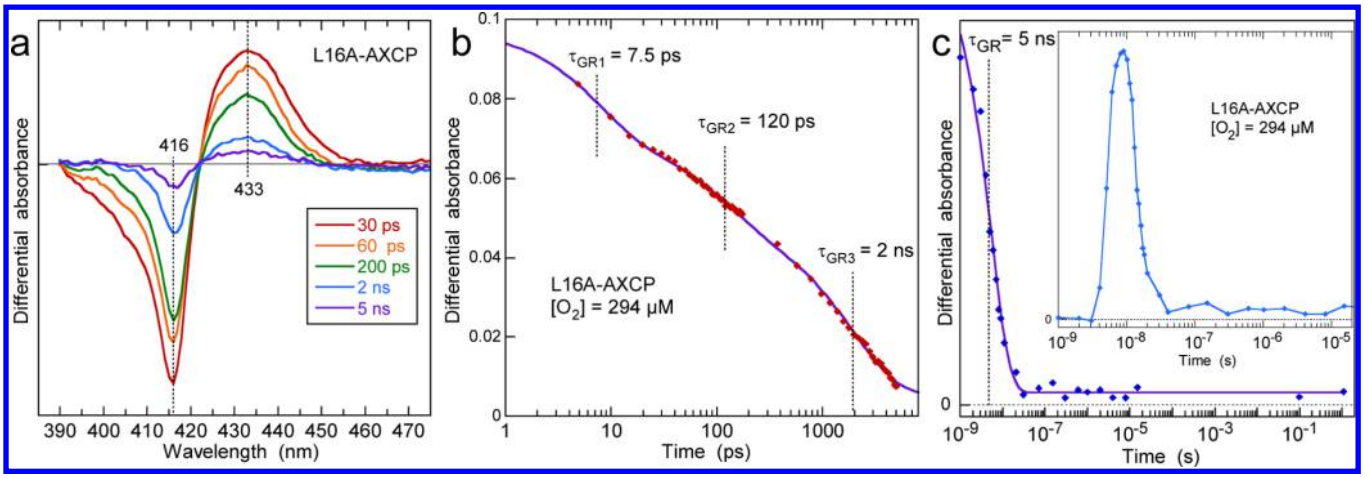

Figure 2. Kinetics of O_2 rebinding to L16A-AXCP from 1 ps to 1 s. (a) Transient absorption spectra at selected time delays after O_2 photodissociation recorded with a 50 fs probe pulse. (b) Kinetics of O_2 rebinding to the heme in the picosecond time range up to 5 ns. The curve is a fit to a function with three exponential decays whose time constants are indicated. The relative amplitudes are given in Table 3. (c) Kinetics of O_2 rebinding to the heme probed at 434 nm in the nanosecond to second time range. The curve is a monoexponential fit. The time origin was set to the maximum of the initial absorption rise. Inset: data showing the initial rise of the signal. The protein was exposed to air: $[O_2]$ = 0.3 mM in solution. T = 20 °C.

accounts for only 6% of the entire NO dynamics after photodissociation, which decompose as a 6 ns component representing ∼6% of the total amplitude (97% of in the nanosecond to millisecond time range) and two other processes (54 ns and 2.8 μs) which account for respectively ∼0.2% and <0.1%. Considering the association constant of NO to L16A-AXCP (k_{on} = 2.9 × 10^6 M^{-1} s^{-1})[26] and the concentration used, [NO] = 200 μM, the bimolecular rebinding constant should appear at ∼1.6 ms (k_{obs} = ∼0.6 × 10^3 s^{-1}) so that the third transition measured at τ_5 = 2.8 μs (A_4 < 0.1%) is not due to bimolecular association but can be assigned either to NO geminate rebinding or to a heme conformational relaxation.

The NO kinetics in the nanosecond to second time range for WT-AXCP dramatically differ from those of L16A-AXCP (Figure 1d). The evolution of the absorbance after 1 ns represents the dynamics of NO, which did not recombine geminately in the picosecond time range, *i.e.*, ∼3% of the photodissociated NO.[20] This measurement displays two processes separated by 6 orders of magnitude in time, each characterized by a rise of the absorption followed by a decay. This behavior is similar to that observed in the case of Sgc,[32] and we put the same interpretation on it. The wavelength at 418 nm corresponds to the 6c-His-NO species of WT-AXCP, and both series of successive rise and decay are assigned to the formation of 6c-His-NO followed by the formation of the 5c-NO species due to the proximal Fe−His bond rupture. The fast one, which appears with very similar time constants (4 ns and 0.25 μs) to those for sGC[32] (4 ns and 0.6 μs), occurs because some NO remains in the core of the protein after dissociation (or was present before). However, the second process due to the bimolecular rebinding occurs more slowly for WT-AXCP (with time constants 25 ms and 0.17 s versus 50 μs and 0.01 s for sGC[32]) even in the presence of 2 mM NO, translating the difference in access to the heme between both proteins. These time constants very closely match those measured earlier with a different spectroscopic system (15 ms and 0.15 s).[19]

Dynamics of Dioxygen. The photodissociation of O_2 from L16A-AXCP gives rise to a bleaching centered at 416 nm and an induced absorption at 433 nm due to the appearance of the ferrous 5c-His heme (Figure 2a), similar to the dissociation of NO. In the picosecond to nanosecond time range, the amplitude of the transient spectrum decreases with a multiexponential behavior (Figure 2b) which indicates different geminate phases of O_2 rebinding. The initial phase (τ_{G1} = 7.5 ps; A_1 = 27.5%) is as fast as the rebinding of NO to the 4c heme of AXCP[20] and is due to O_2, which remains in close proximity to the iron. It is followed by two phases spaced by 1 order of magnitude in time, the second one having the largest relative amplitude (τ_{G2} = 120 ps, A_2 = 22%; τ_{G3} = 2 ns, A_3 = 45%). Importantly, a constant phase whose relative amplitude is 5.2% is revealed, which is assigned to O_2 having left the heme pocket to diffuse into the solvent. Compared with other diatomics, O_2 has a k_{off} more than 10^4 larger than NO and CO, which allows one to observe its escape into the solvent.

To resolve other possible transitions, we also recorded the O_2 dynamics up to 1 s with a highly sensitive detection. Probed at 434 nm, the rise corresponds to the instrument function (Gaussian pulse shape with fwhm ∼5 ns) convoluted with the immediate O_2 dissociation (inset in Figure 2c). The two faster geminate rebinding phases τ_{G1} and τ_{G2} are contained within the pulse width. The subsequent decay, slower than the rise, was fitted to a single exponential with ∼5 ns time constant (Figure 2c) and corresponds to the geminate O_2 rebinding observed previously τ_{G3} = 2 ns, but with a smaller time resolution of the apparatus in this time range. Importantly, there still exists a constant term which does not evolve up to 1 s due to O_2 diffusing into the solvent. We cannot compare these dynamics with those occurring in WT-AXCP, which does not bind O_2, but a comparison can be made with other O_2-binding proteins. The first component of geminate rebinding in L16A-AXCP has a similar time constant and amplitude as the O_2 carrier Mb and the H_2S carrier HbI (Table 2). However, in L16A-AXCP the presence of a third component (τ_3 = 2 ns; A_3 = 45.3 %) considerably decreases the amplitude of O_2 escape (A_4 = 5.2 %), which thus determines the O_2 affinity and leads to a ∼20 times smaller K_D.

Dynamics of Carbon Monoxide. The Soret band of the reduced L16A-AXCP variant appears very sharp after CO binding with a maximum at 418 nm (Figure 3a) and a large

DOI: 10.1021/acschembio.6b00599
ACS Chem. Biol. 2016, 11, 3191−3201

Table 2. Kinetics of O_2 Rebinding to the Mutant L16A-AXCP Compared to Myoglobin and Hemoglobins

		O_2 geminate rebinding			bimolecular rebinding	K_D O_2
protein[a]	ref	τ_1 (A_1)[b]	τ_2 (A_2)	τ_3 (A_3)	A_4 (%)	(M)
L16A - AXCP		7.5 ps (27.5)	120 ps (22)	2 ns (45.3)	5.2	49×10^{-9}
WT Mb	29	6.3 ps (28)	291 ps (6)		65	0.9×10^{-6}
Lp-HbI	29	6.0 ps (20.5)	396 ps (18)		61.5	0.6×10^{-6}

[a]Abbreviations: Mb, myoglobin; *Lp*-Hb, hemoglobin from *Lucina Pectinata*. [b]A_i (%) are the relative amplitudes of each exponential component.

increase of the absorption coefficient. Consequently, the transient spectra after CO photodissociation from L16A-AXCP disclose a pronounced bleach at 416 nm (Figure 3b), similarly to WT-AXCP (Figure 3c) and an induced absorption centered at 434 nm characteristic of the 5c-His ferrous heme.

The amplitude of the transient absorption and bleach rapidly decreases within a few nanoseconds due to CO rebinding and the corresponding kinetics were fitted to a biexponential function (Figure 3d; parameters in Table 3). This behavior for CO sharply contrasts with that observed with myoglobin[33,34] for which only a 180 ns component (4%) was observed. The time constants are about two times slower for L16A-AXCP (τ_{G1} = 543 ps and τ_{G2} = 3.6 ns) than for the WT-AXCP (τ_{G1} = 218 ps and τ_{G2} = 1.9 ns) but with much larger amplitudes and no constant term for the mutant. The remarkable feature of this comparison is the complete CO rebinding for the variant for which the fitted kinetics is illustrated in a logarithmic scale in Figure 3e. Thus, in spite of faster time constants, CO cannot completely rebind to WT-AXCP, as illustrated by the calculated contributions of the CO geminate rebinding without the constant term (Figure 3e). This term represents the proportion of CO which left the interior of the protein and binds bimolecularly from the solvent.

To compare the bimolecular binding for both proteins, we have recorded the dynamics of heme-CO interaction in a very

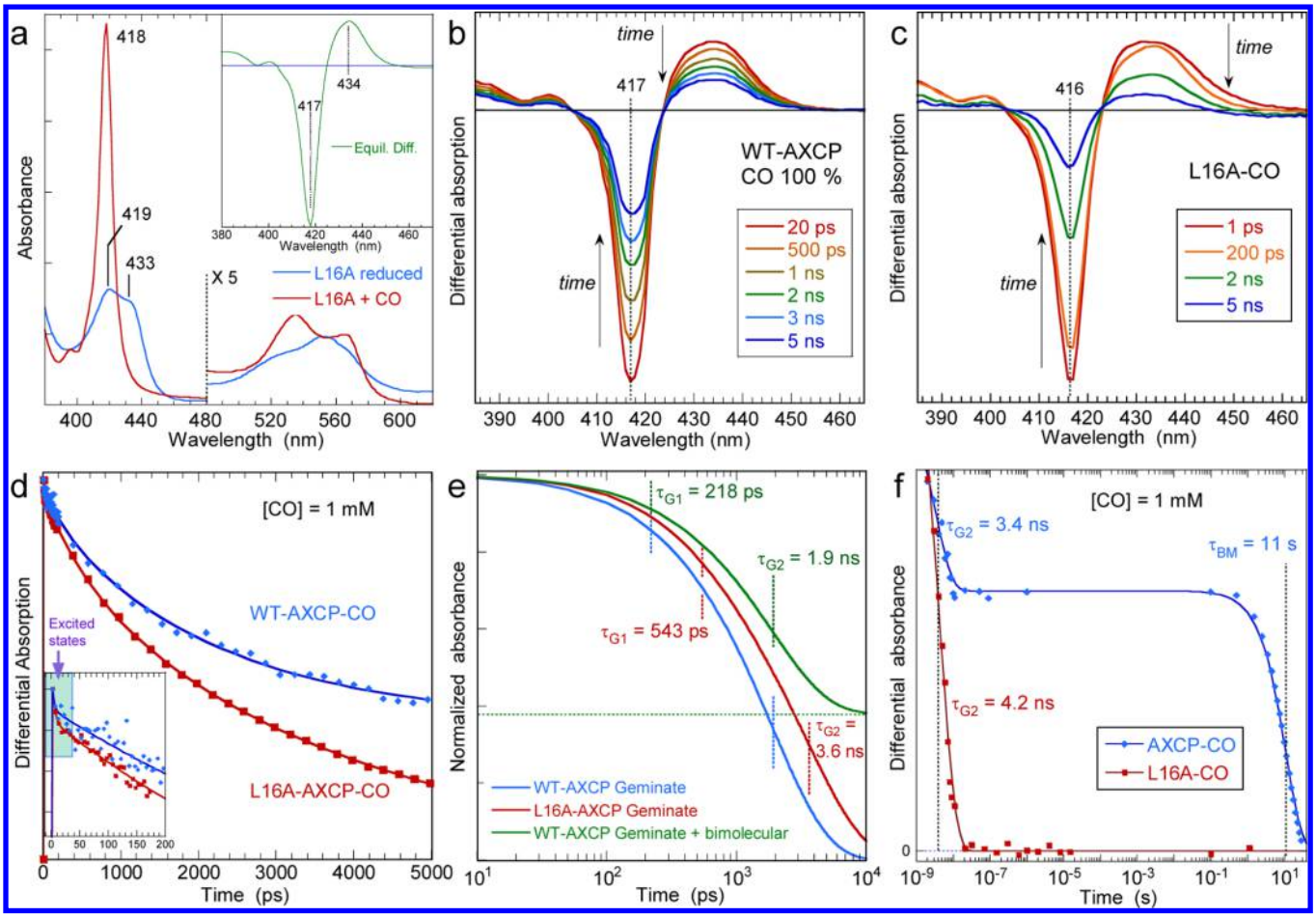

Figure 3. Broad time scale dynamics of CO to WT-AXCP and L16A-AXCP mutant. (a) Equilibrium spectra of ferrous L16A-AXCP unliganded (blue) and CO-liganded (red). Inset: the steady-state difference spectrum. (b) Transient absorption spectra at selected time delays after CO photodissociation from WT-AXCP recorded with a 50 fs probe pulse. (c) Transient absorption spectra for L16A-AXCP-CO. (d) Kinetics of CO rebinding to WT and L16A AXCP in the ps to 5 ns time range. After the initial rise a small decay with τ_{ex} = 4.5 ps is observed, due to the heme excited states relaxation. The curves through data points are fits to biexponential functions. (e) Comparison of normalized calculated contributions of the CO geminate rebinding to WT-AXCP and L16A-AXCP. The blue curve corresponds to the green one without the constant term which represents the bimolecular rebinding. (f) Kinetics of CO rebinding to WT-AXCP and L16A-AXCP probed at 434 nm in the ns to second time range. The curve is a monoexponential fit for L16A-AXCP-CO and a biexponential fit for WT-AXCP-CO. The time origin was set to the maximum of the initial absorption rise. For all data the CO concentration was 1 mM. T = 20 °C.

DOI: 10.1021/acschembio.6b00599
ACS Chem. Biol. 2016, 11, 3191−3201

Table 3. Parameters of CO Rebinding to WT-AXCP and L16A-AXCP Compared with Other Proteins

		CO geminate rebinding			bimolecular rebinding
protein[a]	ref	τ_{4C} (A_1)[b]	τ_{G1} (A_2)	τ_{G2} (A_3)	A_4 (%)
L16A-AXCP	this work		543 ps (18)	3.6 ns (82)	0
WT AXCP	this work		218 ps (4)	1.9 ns (58)	38
sGC	56	6 ps (7)	120 ps (1)	5.7 ns (5)	87
sGC + BAY	56	6 ps (9)	90 ps (20)	1.2 ns (13)	58
Cb-SONO	56	7 ps (5)	100 ps (3)	8.0 ns (8)	84
WT Mb	34			180 ns (4)	96

[a]Abbreviations: sGC: soluble guanylate cyclase. sGC+BAY: soluble guanylate cyclase with bound activator BAY 41−2272. Cb-SONO: sensor of nitric oxide from *Clostridium botulinum*. WT Mb: wild type myoglobin. [b]A_i (%) are the relative amplitudes of each exponential component. The excited state decay (τ_{ex} = 4.5 ps) was not taken into account for calculating the amplitude of CO rebinding phases. τ_{4C} corresponds to the CO rebinding to the 4-coordinate heme.

broad time scale, from 1 ns to 30 s (Figure 3f). It must be again mentioned that, since a fast geminate recombination occurs during the first 4 ns, several cycles of photodissociation and rebinding take place for the very same heme within the pulse duration (5 ns) in this kind of experiment. This explains the apparently larger dissociation yield in the broad time range kinetics (Figure 3f) than in the picosecond to nanosecond range kinetics (Figure 3d). We may note that this effect is smaller than for NO and O_2. The decay, slower than the rise, corresponds to the geminate CO rebinding previously observed. The induced absorbance conspicuously reaches zero for L16A-AXCP at ∼20 ns with a fitted time constant τ_{G2} = 4.1 ns (Figure 3f), corresponding to that measured (τ_{G2} = 3.6 ns) within the picosecond to nanosecond time scale using the 50 fs pulse. Therefore, no other component was detected after 20 ns despite the very high sensibility of our apparatus ($\Delta OD/OD = 10^{-5}$). As for the WT-AXCP, after a 3.4 ns decay, a plateau is reached, which extends for about 8 orders of magnitude in time with no change of the signal amplitude, until the slow bimolecular rebinding of CO to WT-AXCP with a constant τ_{BR} = 11 s. Best measured with a fast pulse (Figure 3d), the amplitude of CO bimolecular rebinding to WT-AXCP represents 38% of photolyzed molecules. Considering the ligand concentration [CO] = 1 mM, this time constant τ_{BR} = 11 s exactly corresponds to the association rate[27] k_{on} = 100 M^{-1} s^{-1}.

Calculated Dynamics of CO. The dynamics of CO within the heme pocket following its dissociation have been calculated up to 500 ps for both WT AXCP and L16A-AXCP. For each protein, 32 trajectories are compared and revealed the salient behavior of CO in the case of the mutant: in all calculated trajectories, the dissociated CO stays at an average distance of 4.2 ± 0.5 Å from the Fe atom (Figure 4), which has itself experienced a fast displacement (in less than 100 fs) toward the proximal heme side of ∼0.3 Å. This average distance of 4.2 Å must be compared with the length of the Fe−CO bond, which is 1.9 Å. For 500 ps, none of the 32 dissociated CO molecules moved farther away. Contrastingly, CO dissociated from the WT AXCP moved away up to 15 Å from the heme Fe in ∼50% of occurrences over 500 ps and even farther than 20 Å in one calculated trajectory. The fact that CO does not move away from Fe explains the absence of any measurable bimolecular rebinding from the solution in the case of L16A-AXCP (Figure 3e−f). Consequently, CO rebinds only geminately from the interior of the heme pocket. There is no steric energy barrier for its motion before binding back to Fe^{2+}, and the time constants (τ_{G1} = 543 ps and τ_{G2} = 3.6 ns) originate only from the need to wait for the Fe atom to be in the heme plane (due to thermal fluctuations) to allow CO binding.[3] Since CO stays at a constant distance from the heme for both monomers of L16A-AXCP (Figure 4b), the presence of two time constants probably originates from conformational fluctuations and not from differences between monomers (because their relative amplitudes are not 50%).

As observed in the superposed structures of WT and L16A-AXCP CO complexes (Figure 4a), the heme conformation of

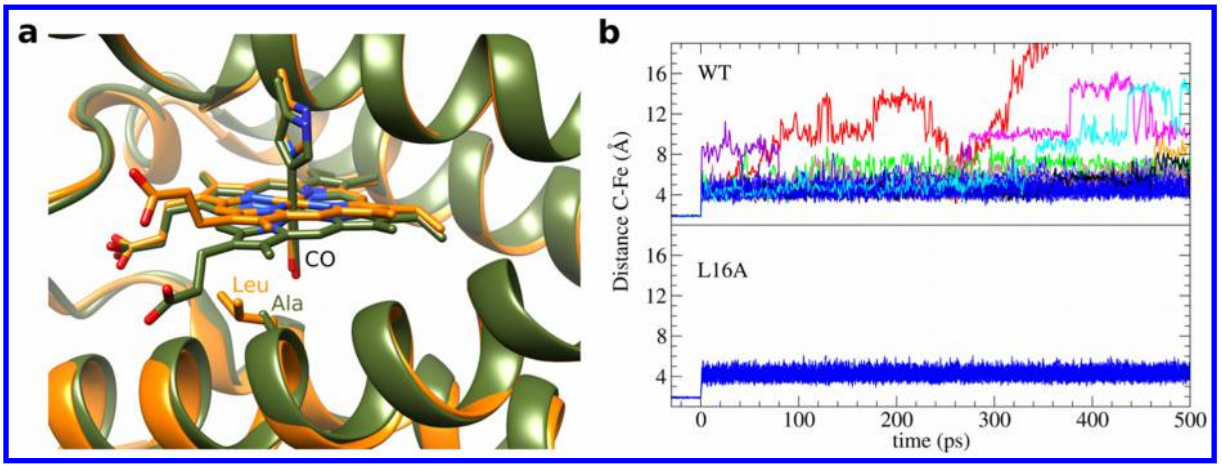

Figure 4. Molecular dynamics calculations. (a) Superposition of the heme pocket structures of WT-AXCP (orange) and L16A-AXCP mutant (green) with bound CO, after energy minimization at 293 K. This figure was generated with Chimera (v1.10.2). (b) Calculated trajectories after CO dissociation for both proteins with the CO position expressed as the distance Fe−C. For both proteins, 32 dynamic trajectories (16 for each monomers) were calculated and are represented here. Structures of both variants with the superposed positions of the center of mass of CO during the 500 ps dynamics are represented in Figures S1−S4.

DOI: 10.1021/acschembio.6b00599
ACS Chem. Biol. 2016, 11, 3191−3201

WT appears distorted, with a propionate side-chain tilted toward the proximal side. We must note that two possible conformations of the heme in WT-AXCP-CO are clearly resolved in the crystal structures at 100 K.[27] They differ from each other by the orientation of the Fe−C−O unit, which can be bent, with both heme propionates directed toward the distal side, or linear, with one propionate directed toward the proximal side. The Raman spectrum of WT-AXCP-CO allowed the identification of the presence of both conformations at 100 K, but only one in solution at 293 K, namely the linear Fe−C−O unit associated with one propionate tilted toward the proximal side.[27] We measured all absorption kinetics at 293 K and consequently selected this latter structure of WT-AXCP-CO for energy minimization (Figure 4a). During the entire computed energy minimization process, the proximally tilted propionate kept its orientation.

The smaller Ala side-chain does not bring supplementary steric constraints with respect to Leu, and no other structural changes occurred.[27] The potential well in which CO is held in the L16A variant is induced by its heme conformation and the space freed by smaller Ala and constrained by the propionate.

Internal Dynamics and Affinity. We discuss here the origins of the drastic changes in ligand dynamics, then the relationship between these dynamics and the kinetic rates determining the affinity. During past decades, a large number of mutations in the distal pocket of heme proteins, including Leu and Ala, were evaluated for their role on diatomic dynamics and affinity, mostly performed on Mb,[1,7−9,34−39] but also on peroxidase[11] and hemoglobins from invertebrates.[40,41] This large amount of data allowed general features of the protein−diatomic interaction to be inferred, and we must compare AXCP-L16A data with the Leu ↔ Ala substitutions in Mb, direct (such as L29A) or indirect (such as H64L versus H64A).

The largest changes observed in Mb are ∼100 to 700-fold increases of $k_{off}(O_2)$ due to the removal of the stabilizing H-bond of His64 (H64V or H64W),[37,42] whereas other mutations change k_{on} and k_{off} by factors ≤100. Now, if we compare the effects of all distal pocket Ala↔Leu replacements, whatever their position in the ligand pathway, the rates change only by a factor ≤ 7 for CO (k_{off}(CO), did not even change for L29A in Mb) and only 3-fold for O_2 (refs 33−40). At position 64 in Mb (the so-called "E7-gate"), the size effects of H64L versus H64A are limited for O_2: k_{on} and k_{off} increased respectively 2-fold and 4-fold[43] but appear larger for CO: k_{on}(CO) decreased 6-fold[36,38] and k_{off}(CO) increased 2.5-fold leading to a 16-fold decrease of CO affinity[36] due to an 18-fold increased rebinding yield,[44] which has been explained by a favorable hydrophobicity for CO.[44]

Leu29 is located very close to bound O_2, on the pathway to the Xe4 site, associated with the "C-states" of docked O_2, whereas His64 is located on the pathway from the solvent to the distal heme pocket.[37,43] The mutation L29A in Mb changes neither the O_2 affinity, nor its bimolecular binding rates, nor the total amplitude (fast + slow) of its geminate rebinding,[37] although it changed the rate of the picosecond phase.[43] This mutation in Mb induces the same effects on NO geminate and binding rates, keeping unchanged the NO affinity,[43] affecting essentially the docking site. Contrastingly, the L16A mutation in AXCP induced a high O_2 affinity ($K_D(O_2)$ = 49 nM; $K_D(O_2)$ = ∼ 1 μM fo Mb) from the strict absence of O_2 binding in WT-AXCP (predicted 10^8-fold increase of $K_D(O_2)$!).[13] In the second shell of side-chains surrounding the distal heme pocket in Mb, the mutation L32A changed the rates by a factor of 2, not affecting the O_2 affinity.[43]

In a different ligand pathway, the apolar tunnel in the globin from sea worm *Cerebratulus lacteus* single substitutions probing the residue size effect (A55L and L86A) led to a parallel increase or decrease of rates[40] with factors in the range 2−10 for O_2 and 1.1−5 for NO.[40] These Leu ↔ Ala replacements in the globin family nicely exemplify the effects of the size of residues on the dynamics of diatomics from and to the sites along their pathway. Overall, changing the steric hindrance on the ligand pathway results in the simultaneous increase of both *on* and *off* rates or a decrease of both rates. In the case of L16A-AXCP, the mere exchange from Leu to Ala simultaneously induces a 10^4-fold k_{on} increase and a 10^4-fold k_{off} decrease for CO (10^8-fold decrease of K_D(CO)) which cannot be due solely to a change of steric barrier for CO diffusion. Similarly, for NO k_{on} increased while k_{off} decreased, both by several orders of magnitude, pointing out a mechanism different than the release of steric hindrance. Here, the side chain Ala16 does not act directly on diatomics but allows the prioponate heme chain to adopt a new conformation, trapping the ligand. So far, such a mechanism was not observed in other metalloproteins, but it may explain the very high affinities of the three diatomics for soybean leghemoglobin,[45] similar to those for L16A-AXCP and associated with a high picosecond geminate yield.[46]

The discrimination between NO and CO in 5c-His heme proteins is governed by their electronic configurations: NO possesses an unpaired electron whereas CO has a pair of electrons, resulting in a high enthalpic barrier for CO binding but a negligeable one for NO.[2,3] This difference results in the possibility for NO to bind to Fe^{2+} positioned out of the heme plane,[3−5] whereas CO must wait for favorable fluctuations of the heme to become close to an in-plane conformation. In L16A-AXCP, the binding of trapped CO is only limited by the thermal Fe^{2+} motion in the heme plane, inducing an extremely high CO rebinding yield (∼100%). Formally, the CO escape to solvent cannot be zero, but it is not detectable (≪ 0.5%). Contrastingly, CO only partially rebinds to WT-AXCP (62%) with no phase during eight time decades until the slow bimolecular rebinding from solvent. The L16A mutation precludes the diffusion of the diatomic out of the heme pocket, so that an extremely low number of molecules can reach the exterior of the protein, giving rise to k_{off}(CO) in days.[27,47]

Although the overall heme−CO dissociation constant for WT-AXCP (K_D = 2.6 × 10^{-4} M) is similar to that for sGC, both the *on* and *off* rate constants of WT-AXCP are lower by a factor of 400, demonstrating the existence of a steric barrier for CO in WT-AXCP with respect to sGC. Whereas the L16A mutation decreases k_{off} for both CO and NO by the same order of magnitude (∼10^4), their corresponding k_{on}'s increase differently by factors of 10^4 and 10^2, respectively, to reach similar values (separated by a factor of 2.6). Again, such a behavior cannot be induced by the simple release of a steric hindrance but agrees with a difference of probability of reaction between Fe^{2+} and CO or NO induced by a heme pocket conformational change. The heme propionate closest to Leu16, oriented toward the proximal heme face in WT-AXCP but toward the distal heme face in L16A mutant (Figure S3), controls the dynamics. According to the calculated dynamics (Figures S1−S3 and supplementary movie), CO moves in WT-AXCP through a pathway which is occupied by the propionate in L16A-AXCP. The space freed by the smaller Ala constitutes a trapping site, constrained by the distally oriented propionate,

DOI: 10.1021/acschembio.6b00599
ACS Chem. Biol. 2016, 11, 3191−3201

Table 4. Kinetic Parameters for 6c-NO and 6c-CO Complexes of L16x AXCP Variants

protein	k_{on} NO (M^{-1} s^{-1})	k_{off} NO (s^{-1})	K_D NO (M)	k_{on} CO (M^{-1} s^{-1})	k_{off} CO (s^{-1})	K_D CO (M)	ref
WT AXCP	4.4×10^{4}[a]	6×10^{-3}[a]	1.4×10^{-7}[a]	101	2.8×10^{-2}	2.8×10^{-4}	26, 47
L16A	2.9×10^{6}	2×10^{-7}	6.9×10^{-14}	1.1×10^{6}	3.7×10^{-6}	3.4×10^{-12}	26, 27
L16G	nd[b]	nd	nd	5×10^{5}	7.4×10^{-6}	1.5×10^{-11}	26, 27
sGC 6c-XO	4.5×10^{8}	27	1.7×10^{-7}	4×10^{4}	10.7	2.6×10^{-4}	1, 50
sGC 5c-NO[c]	1.4×10^{8}	6×10^{-4}	4.3×10^{-12}				32, 50
heme model	1.8×10^{8}	2.9×10^{-4}	1.6×10^{-12}	1.1×10^{7}	2.5×10^{-2}	2.3×10^{-9}	57, 58
Mb	2.2×10^{7}	1×10^{-4}	4.5×10^{-12}	5.1×10^{5}	1.9×10^{-2}	3.7×10^{-8}	42

[a]First step of NO binding. The k_{off} for 5c-NO AXCP is not determined. [b]Not yet determined. [c]Transient species.

from where CO can exit only by moving in the interaction sphere of the iron orbitals. As a result, the heme reactivity increases and so does k_{on}(CO) by 10^4 due to CO trapping close to the iron. As for NO, despite its trapping close to the iron, its k_{on} increased by only $\sim 10^2$ because NO has already a high reactivity toward the heme, whatever its configuration.

In the upper nanosecond time range, the geminate rebinding phases are due to diatomic ligands located in the protein core but not within the heme pocket.[38,48,49] Some mutations of Mb provoke the appearance of such phases for CO geminate rebinding[34,38] with varying amplitudes up to 57%, but always with time constants in the range 60−230 ns (compared to 180 ns, 4% for WT Mb).[33,34] As for Mb-O_2, a 60 ns component (~40%) exists in WT and in mutants.[34] In the case of L16A-AXCP, we did not observe a component in the time range extending from 5×10^{-8} to 10^{-1} s, whatever the diatomic (only a 54 ns component for NO with amplitude <0.5%) until bimolecular rebinding. Again, this implies that diatomics are not in a docking site but trapped in the heme pocket and forced to stay close to the heme, as demonstrated by molecular dynamics calculations (Figure 4b, Figures S1−S3).

In the picosecond time range, the NO geminate rebinding to the L16A-AXCP mutant appears biexponential, like all 6-coordinate NO-heme (6c-NO) proteins, but is the most efficient (94%) ever measured in 6c-NO hemes. Albeit the faster time constant is similar to those of myoglobin and NO-synthase (Table 1), its relative amplitude (13.9 ps; 67%) is predominant, with no measurable exit of NO from the protein. These dynamics originate from the confinement of NO in the distal heme pocket of L16A-AXCP and are directly translated into a very low k_{off} (Table 4). On the nanosecond to second time scale, no component assigned to bimolecular rebinding can be observed, in contrast with 5c-NO WT-AXCP and sGC for which a single fast component is measured (7.5 ps; 97%) together with an observable bimolecular rebinding (~3−4%).[50] A pertinent comparison is made with the 6c-NO WT-AXCP (stabilized at very low NO concentration),[20] where NO is bound to the distal heme side, similarly with L16A-AXCP, which presents a single picosecond geminate rebinding (52 ps; 43%) whose larger time constant and lower amplitude compared to L16A-AXCP are due to the position of NO which is not trapped close to the heme.

The very fast geminate NO rebinding to the 4c-heme in sGC[50] and in isolated heme is correlated with a NO k_{off} rate (6×10^{-4} and 2.9×10^{-4} s^{-1}, respectively) which is 1 order of magnitude smaller than the k_{off} rate from the distal side in 6c-NO WT-AXCP (6×10^{-3} s^{-1}).[47] In 5c-NO proteins, k_{off} is mainly determined by the reactivity of the 4c-heme, whereas in 6c-NO proteins k_{off} is mainly determined by the partitioning between the heme pocket and the channel to solvent, controlled by steric barriers. Saliently, the trapping of diatomics very closely to the heme iron appears here as another mechanism, at the origin of the very low k_{off} in 6c-NO L16A-AXCP, 3 orders of magnitude lower than for sGC.

The first component of O_2 geminate rebinding (τ_1 = 7.5 ps; A_1 = 27.5%) is remarkably similar to that of Mb-O_2, both in amplitude and in time constant. However, the overall O_2 rebinding to L16A-AXCP appears much more efficient (~95%) than to Mb (~35%) as a consequence of the considerably decreased proportion of O_2 exiting the distal heme pocket (5.2% versus 65%) revealing again a trapping of O_2 in L16A-AXCP. There is no H-bond in the distal heme pocket[27] which would stabilize bound O_2, indicating that only factors at the heme level intervene in the decrease of the k_{off} rate.

The effects of L16A mutation are not limited to ligand dynamics: the comparison of the X-ray structures of WT- and L16A-CO complexes (Figure 4a) indicates a change of conformation which releases a strain exerted on the heme with deep consequences: its redox potential increases by ~400 mV with respect to WT-AXCP,[27] and the binding of NO no longer triggers the Fe-His bond cleavage (Figure 1).

In conclusion, the mutation L16A confers to the heme pocket of AXCP the ability to trap diatomics within very close distance from the Fe^{2+}, so that the probability of rebinding after dissociation (either photoactivated or thermal) is maximized and the probability of escape from the protein is minimized. The dynamics over 12 time decades demonstrates that the affinity of the Fe^{2+}-XO 6-coordinate distal complex in L16A-AXCP is governed by the distal heme pocket which forces the diatomics to stay in the interaction volume of the heme iron due to the distal position of the propionate close to Ala16. This most favorable distal heme conformation traps and forces the diatomic ligands CO, NO, and O_2 to rebind in an ultrafast manner with extremely high yield, a unique property among heme proteins, which is directly translated into a very high affinity toward L16A-AXCP.

METHODS

Preparation of the Samples. Cytochrome *c′* from *Alcaligenes xylosoxidans* and its L16A mutant were expressed and purified as already described.[27] The solution of ferric WT or L16A-AXCP (100 μL, 50 μM in 10 mM TEA buffer, pH 7.4) was put in a 1 mm optical path length quartz cell sealed with a rubber stopper and degassed by means of four successive cycles of vacuum (0.3 mbar) and purging with pure argon (1.3 bar) for 15 min between each cycles. The ferrous heme was obtained by the addition of 10 μL of degassed sodium ascorbate solution (2 mM final concentration) which should eliminate remaining O_2. For preparing ferrous NO-liganded AXCP, gas phase 100% NO or 10% in N_2 (Air Liquide) was directly introduced into the spectroscopic cell (total pressure of 1.3 bar, yielding 2 mM and 200 μM of NO in the aqueous phase respectively). Equilibrium spectra were recorded at each step for monitoring the coordination state by

DOI: 10.1021/acschembio.6b00599
ACS Chem. Biol. 2016, 11, 3191−3201

the evolution of Soret band. The absorbance (UV-1700 Shimadzu spectrometer) of the sample was in the range 0.5−0.8 at the Soret maximum for 1 mm path length.

Picosecond Time-Resolved Absorption Spectroscopy. Picosecond absorption spectroscopy was performed with the pump−probe laser system previously described.[51] The photodissociation of NO was achieved with an excitation pulse at 564 nm, in the Q-band absorption, whose duration was ∼40 fs with a repetition rate of 30 Hz. The probe pulse generated from a continuum had a broad spectrum pulse (375−500 nm), and the transient Soret absorption was recorded as a function of delay between pump and probe pulses. The optical path length of the cell was 1 mm. The sample was continuously moved perpendicularly to the laser beam, and the temperature was 20 °C. Transient spectra were recorded with a CCD detector simultaneously to the kinetics as time-wavelength matrix data. Analysis of the data was performed by singular value decomposition (SVD)[51,52] of the time-wavelength matrix such that all transient spectral components were identified in the time window 0.5 ps to 5 ns. Up to 40 scans were recorded and averaged with a dwell time of 1 s at each individual transient spectrum. The SVD kinetic components associated with SVD spectral components were fitted to the sum of a minimum number of exponential components. Alternatively, kinetics were also performed at particular wavelengths of the raw data matrix.

Nanosecond to Millisecond Time-Resolved Absorption. For this extended time range, we have used a home-built spectrophotometer comprising two lasers which are electronicly synchronized.[31] The dissociating pulse is provided by the second harmonic (532 nm) of a Nd/YAG laser and has a duration of 6 ns. The probing pulses (5 ns fwhm) were provided by a tunable optical parametric oscillator pumped by the third harmonic of a Nd/YAG laser (Continuum). The sample cell compartment and light collection design allowed us to record signal variations ΔOD/OD as low as 10^{-5}. The kinetics of differential absorption changes were probed at particular wavelengths by tuning the OPO. Up to 12 scans were averaged for each kinetics. Time delay after the dissociating pulse was changed linearly from 1 to 30 ns, then was changed with a logarithmic progression from 30 ns to 1 s. The kinetics at different wavelengths were globally fitted by using the same time constants at all wavelengths.

Molecular Dynamics Simulation Protocol. We constructed WT and L16A dimer models of *Achromobacter xylosoxidans* cytochrome *c*′, using the same simulation protocol with the PDB crystal structures files code 2YLD and 2YLG.[27] All molecular dynamic simulations were performed with the program CHARMM[53] version 39. Electrostatic interactions were computed with the Particle Mesh Ewald method and periodic boundary conditions were used. Nonbonding interactions were smoothly decreased to zero between 10 and 12 Å, and a dielectric constant equal to unity was used. All bonds with hydrogen atoms were constrained using the SHAKE algorithm. The AXCP model was solvated using a rhombic dodecahedron water box shape with a 76 Å edge length and neutralized with potassium and chloride ions at 0.15 M concentration. After energy minimization using 200 SD steps and 2500 ABNR steps, the AXCP structures were heated to 310 K and equilibrated with periodic assignment of velocities every 1 ps. The equilibration phase duration varies from 1.25 to 3 ns in order to generate eight independent trajectories. Free dynamics over 250 and 500 ps were performed before 500 ps CO ligand dissociation simulations. To simulate the dissociation, the bond between heme iron and ligand was deleted and liganded parameters switched to unliganded parameters at the two heme sites simultaneously. This method produces an energy excess on the same order of magnitude as the photon energy used to photodissociate the CO ligand in the experiment. The unliganded CO was simulated using a three charge model.[54] The ligand recombination process was not treated in these simulations since we aimed at determining the motion of CO within the heme pocket. The leapfrog verlet integrator with a 1 fs time step was used, and the structure was saved every 1 ps for analysis. The root-mean-square deviation of backbone atoms of the WT and L16A trajectories remains below 3 Å.

■ ASSOCIATED CONTENT

Supporting Information

The Supporting Information is available free of charge on the ACS Publications website at DOI: 10.1021/acschembio.6b00599.

Figures S1 to S3: calculated trajectories of CO in AXCP variants (PDF)

Movie showing the exit pathway of CO in WT AXCP (AVI)

■ AUTHOR INFORMATION

Corresponding Author

*Tel: 331 69 33 50 52. E-mail: michel.negrerie@polytechnique.fr.

Notes

The authors declare no competing financial interest.

■ ACKNOWLEDGMENTS

This work was supported by National Science Foundation Grants MCB-0745035 and MCB-1411963 (to C.R.A.). We thank S. Antonyuk, R. Eady, and S. Hasnain for providing AXCP samples.

■ DEDICATION

Dr. F. Rappaport passed away on January 12th, 2016, during the writing of the manuscript. This article is dedicated to his memory.

■ REFERENCES

(1) Tsai, A.-L., Berka, V., Martin, E., and Olson, J. S. (2012) A sliding scale rule for selectivity among NO, CO, and O_2 by heme protein sensors. *Biochemistry 51*, 172−186.

(2) Franzen, S. (2002) Spin-dependent mechanism for diatomic ligand binding to heme. *Proc. Natl. Acad. Sci. U. S. A. 99*, 16754−16759.

(3) Ionascu, D., Gruia, F., Ye, X., Yu, A. C., Rosca, F., Beck, C., Demidov, A., Olson, J. S., and Champion, P. M. (2005) Temperature-dependent studies of NO recombination to heme and heme proteins. *J. Am. Chem. Soc. 127*, 16921−16934.

(4) Ye, X., Ionascu, D., Gruia, F., Yu, A., Benabbas, A., and Champion, P. M. (2007) Temperature-dependent heme kinetics with nonexponential binding and barrier relaxation in the absence of protein conformational substates. *Proc. Natl. Acad. Sci. U. S. A. 104*, 14682−14687.

(5) Kruglik, S. G., Yoo, B.-K., Franzen, S., Vos, M. H., Martin, J.-L., and Negrerie, M. (2010) Picosecond primary structural transition of the heme is retarded after nitric oxide binding to heme proteins. *Proc. Natl. Acad. Sci. U. S. A. 107*, 13678−13783.

(6) Spiro, T. G., Zgierski, M. Z., and Kozlowski, P. M. (2001) Stereoelectronic factors in CO, NO and O_2 binding to heme from vibrational spectroscopy and DFT analysis. *Coord. Chem. Rev. 219*, 923−936.

(7) Olson, J. S., and Phillips, G. N., Jr. (1997) Myoglobin discriminates between O_2, NO, and CO by electrostatic interactions with the bound ligand. *JBIC, J. Biol. Inorg. Chem. 2*, 544−552.

(8) Quillin, M. L., Li, T. S., Olson, J. S., Phillips, G. N., Jr., Duo, Y., Ikeda-Saito, M., Regan, R., Carlson, M., Gibson, Q. H., Li, H. Y., and Elber, R. (1995) Structural and functional effects of apolar mutations of the distal valine in myoglobin. *J. Mol. Biol. 245*, 416−436.

(9) Draghi, F., Miele, A. E., Travaglini-Allocatelli, C., Vallone, B., Brunori, M., Gibson, Q. H., and Olson, J. S. (2002) Controlling ligand binding in myoglobin by mutagenesis. *J. Biol. Chem. 277*, 7509−7519.

(10) Dou, Y., Maillett, D. H., Eich, R. F., and Olson, J. S. (2002) Myoglobin as a model system for designing heme protein based blood substitutes. *Biophys. Chem. 98*, 127−148.

DOI: 10.1021/acschembio.6b00599
ACS Chem. Biol. 2016, 11, 3191−3201

(11) Rodriguez-Lopez, J. N., Smith, A. T., and Thorneley, R. N. (1997) Effect of distal cavity mutations on the binding and activation of oxygen by ferrous horseradish peroxidase. *J. Biol. Chem. 272*, 389−395.
(12) Murphy, E. J., Marechal, A., Segal, A. W., and Rich, P. R. (2010) CO binding and ligand discrimination in human myeloperoxidase. *Biochemistry 49*, 2150−2158.
(13) Tsai, A.-L., Martin, E., Berka, V., and Olson, J. S. (2012) How do heme-protein sensors exclude oxygen? Lessons learned from cytochrome *c′*, *Nostoc puntiforme* heme nitric oxide/oxygen-binding domain, and soluble guanylyl cyclase. *Antioxid. Redox Signaling 17*, 1246−1263.
(14) Hough, M. A., and Andrew, C. R. (2015) Cytochromes c′: structure, reactivity and relevance to haem-based gas sensing. *Adv. Microb. Physiol. 67*, 1−84.
(15) Cross, R., Aish, J., Paston, S. J., Poole, R. K., and Moir, J. W. B. (2000) Cytochrome *c′* from *Rhodobacter capsulatus* confers increased resistance to nitric oxide. *J. Bacterial. 182*, 1442−1447.
(16) Cross, R., Lloyd, D., Poole, R. K., and Moir, J. W. B. (2001) Enzymatic removal of nitric oxide catalyzed by cytochrome *c′* in *Rhodobacter capsulatus*. *J. Bacteriol. 183*, 3050−3054.
(17) Mayburd, A., and Kassner, R. J. (2002) Mechanism and biological role of nitric oxide binding to cytochrome *c′*. *Biochemistry 41*, 11582−11591.
(18) Choi, P. S., Grigoryants, V. M., Abruña, H. D., Scholes, C. P., and Shapleigh, J. P. (2005) Regulation and function of cytochrome *c′* in *Rhodobacter sphaeroides* 2.4.3. *J. Bacteriol. 187*, 4077−4085.
(19) Andrew, C. R., Rodgers, K. R., and Eady, R. R. (2003) A novel kinetic trap for NO release from cytochrome c′: a possible mechanism for NO release from activated soluble guanylate cyclase. *J. Am. Chem. Soc. 125*, 9548−9549.
(20) Yoo, B.-K., Lamarre, I., Martin, J.-L., Andrew, C., and Negrerie, M. (2013) Picosecond binding of the His ligand to four-coordinate heme in cytochrome c′: a one-way gate for releasing proximal NO. *J. Am. Chem. Soc. 135*, 3248−3254.
(21) Andrew, C. R., George, S. J., Lawson, D. M., and Eady, R. R. (2002) Six- to five-coordinate heme-nitrosyl conversion in cytochrome c′ and its relevance to guanylate cyclase. *Biochemistry 41*, 2353−2360.
(22) Lawson, D. M., Stevenson, C. E. M., Andrew, C. R., and Eady, R. R. (2000) Unprecedented proximal binding of nitric oxide to heme: implications for guanylate cyclase. *EMBO J. 19*, 5661−5671.
(23) Nioche, P., Berka, V., Vipond, J., Minton, N., Tsai, A.-L., and Raman, C. S. (2004) Femtomolar sensitivity of a NO sensor from *Clostridium botulinum*. *Science 306*, 1550−1553.
(24) Pellicena, P., Karow, D., Boon, E., Marletta, M., and Kuriyan, J. (2004) Crystal structure of an oxygen-binding heme domain related to soluble guanylate cyclases. *Proc. Natl. Acad. Sci. U. S. A. 101*, 12854−12859.
(25) Herzik, M. A., Jonnalagadda, R., Kuriyan, J., and Marletta, M. A. (2014) Structural insights into the role of iron-histidine bond cleavage in nitric oxide-induced activation of H-NOX gas sensor proteins. *Proc. Natl. Acad. Sci. U. S. A. 111*, E4156−E4164.
(26) Garton, M. E., Pixton, D. A., Petersen, C. A., Eady, R. R., Hasnain, S. S., and Andrew, C. R. (2011) A distal pocket Leu residue inhibits the binding of O_2 and NO at the distal heme site of cytochrome c′. *J. Am. Chem. Soc. 134*, 1461−1463.
(27) Antonyuk, S. V., Rustage, N., Petersen, C. A., Arnst, J. L., Heyes, D. J., Sharma, R., Berry, N. G., Scrutton, N. S., Eady, R. R., Andrew, C. R., and Hasnain, S. S. (2011) Carbon monoxide poisoning is prevented by the energy costs of conformational changes in gas-binding haemproteins. *Proc. Natl. Acad. Sci. U. S. A. 108*, 15780−15785.
(28) Andrew, C. R., Green, E. L., Lawson, D. M., and Eady, R. R. (2001) Resonance Raman spectra of cytochrome c′ and its relevance to guanylate cyclase. *Biochemistry 40*, 4115−4122.
(29) Ramos-Alvarez, C., Yoo, B.-K., Pietri, R., Lamarre, I., Martin, J.-L., Lopez-Garriga, J., and Negrerie, M. (2013) Reactivity and dynamics of H_2S, NO and O_2 interacting with hemoglobins from *Lucina pectinata*. *Biochemistry 52*, 7007−7021.
(30) Russell, H. J., Hardman, S. J., Heyes, D. J., Hough, M. A., Greetham, G. M., Towrie, M., Hay, S., and Scrutton, N. S. (2013) Modulation of ligand-heme reactivity by binding pocket residues demonstrated in cytochrome c′ over the femtosecond−second temporal range. *FEBS J. 280*, 6070−6082.
(31) Beal, D., Rappaport, F., and Joliot, P. (1999) A new high-sensitivity 10-ns time-resolution spectrophotometric technique adapted to in vivo analysis of the photosynthetic apparatus. *Rev. Sci. Instrum. 70*, 202−207.
(32) Yoo, B.-K., Lamarre, I., Martin, J.-L., Rappaport, F., and Negrerie, M. (2015) Motion of proximal histidine and structural allosteric transition in soluble guanylate cyclase. *Proc. Natl. Acad. Sci. U. S. A. 112*, E1697−E1704.
(33) Henry, E. R., Sommer, J. H., Hofrichter, J., Eaton, W. A., and Gellert, M. (1983) Geminate recombination of carbon monoxide to myoglobin. *J. Mol. Biol. 166*, 443−451.
(34) Huang, X., and Boxer, S. G. (1994) Discovery of new ligand binding pathways in myoglobin by random mutagenesis. *Nat. Struct. Biol. 1*, 226−229.
(35) Ikeda-Saito, M., Dou, Y., Yonetani, T., Olson, J. S., Li, T. S., Regan, R., and Gibson, Q. H. (1993) Ligand diffusion in the distal heme pocket of myoglobin: a primary determinant of geminate rebinding. *J. Biol. Chem. 268*, 6855−6857.
(36) Li, T., Quillin, M. L., Phillips, G. N., and Olson, J. S. (1994) Structural determinants of the stretching frequency of CO bound to myoglobin. *Biochemistry 33*, 1433−1446.
(37) Scott, E. E., Gibson, Q. H., and Olson, J. S. (2001) Mapping the pathways for O_2 entry into and exit from myoglobin. *J. Biol. Chem. 276*, 5177−5188.
(38) Sugimoto, T., Unno, M., Shiro, Y., Dou, Y., and Ikeda-Saito, M. (1998) Myoglobin mutants giving the largest geminate yield in CO rebinding in the nanosecond time domain. *Biophys. J. 75*, 2188−2194.
(39) Uchida, T., Ishimori, K., and Morishima, I. (1997) The effects of heme pocket hydrophobicity on the ligand binding dynamics in myoglobin as studied with leucine 29 mutants. *J. Biol. Chem. 272*, 30108−30115.
(40) Salter, M. D., Blouin, G. C., Soman, J., Singleton, E. W., Dewilde, S., Moens, L., Pesce, A., Nardini, M., Bolognesi, M., and Olson, J. S. (2012) Determination of ligands pathways in globins: apolar tunnels versus polar gates. *J. Biol. Chem. 287*, 33163−33178.
(41) Nienhaus, K., Knapp, J. E., Palladino, P., Royer, W., and Nienhaus, U. (2007) Ligand migration and binding in the dimeric hemoglobin of *Scapharca inaequivalvis*. *Biochemistry 46*, 14018−14031.
(42) Springer, B. A., Sligar, S. G., Olson, J. S., and Phillips, G. N. (1994) Mechanisms of ligand recognition in myoglobin. *Chem. Rev. 94*, 699−714.
(43) Gibson, Q. H., Regan, R., Elber, R., Olson, J. S., and Carver, T. E. (1992) Distal pocket residues affect picosecond ligand recombination in myoglobin. *J. Biol. Chem. 267*, 22022−22034.
(44) Sakan, Y., Ogura, T., Kitagawa, T., Fraunfelter, F. A., Mattera, R., and Ikeda-Saito, M. (1993) Time-resolved resonance Raman study on the binding of carbon monoxide to recombinant human myoglobin and its distal histidine mutants. *Biochemistry 32*, 5815−5824.
(45) Hargrove, M. S., Barry, J. K., Brucker, E. A., Berry, M. B., Phillips, G. N., Olson, J. S., Arredondo-Peter, R., Dean, J. M., Klucas, R. V., and Sarath, G. (1997) Characterization of recombinant soybean leghemoglobin a and apolar distal histidine mutants. *J. Mol. Biol. 266*, 1032−1042.
(46) Chowdhury, P. K., Kundu, S., Halder, M., Das, K., Hargrove, M. S., and Petrich, J. W. (2003) Effects of distal pocket mutations on the geminate recombination of NO with leghemoglobin on the pico-second time scale. *J. Phys. Chem. B 107*, 9122−9127.
(47) Pixton, D. A., Petersen, C. A., Franke, A., van Eldik, R., Garton, E. M., and Andrew, C. R. (2009) Activation parameters for heme-NO binding in *Alcaligenes xylosoxidans* cytochrome c′: the putative dinitrosyl intermediate forms via a dissociative mechanism. *J. Am. Chem. Soc. 131*, 4846−4853.

DOI: 10.1021/acschembio.6b00599
ACS Chem. Biol. 2016, 11, 3191−3201

(48) Ansari, A., Jones, C. M., Henry, E. R., Hofrichter, J., and Eaton, W. A. (1994) Conformational relaxation and ligand binding in myoglobin. *Biochemistry 33*, 5128−5145.
(49) Negrerie, M., Berka, V., Vos, M. H., Liebl, U., Lambry, J.-C., Tsai, A.-L., and Martin, J.-L. (1999) Geminate recombination of nitric oxide to endothelial nitric oxide-synthase and mechanistic implications. *J. Biol. Chem. 274*, 24694−24702.
(50) Yoo, B.-K., Lamarre, I., Martin, J.-L., and Negrerie, M. (2012) Quaternary structure controls ligand dynamics in soluble guanylate cyclase. *J. Biol. Chem. 287*, 6851−6859.
(51) Negrerie, M., Cianetti, S., Vos, M. H., Martin, J. L., and Kruglik, S. G. (2006) Photoinduced coordination dynamics of cytochrome *c*: ferrous versus ferric species studied by time-resolved resonance Raman and transient absorption spectroscopies. *J. Phys. Chem. B 110*, 12766−12781.
(52) Vandegriff, K. D., and Shrager, R. I. (1994) Hemoglobin-oxygen equilibrium binding − Rapid-scanning spectrophotometry and singular-value decomposition. *Methods Enzymol. 232*, 460−485.
(53) Brooks, B. R., Bruccoleri, R. E., Olafson, B. D., Swaminathan, S., Karplus, M., and States, D. J. (1983) CHARMM: a program for macromolecular energy, minimisation, and dynamics calculations. *J. Comput. Chem. 4*, 187−217.
(54) Straub, J. E., and Karplus, M. (1991) Molecular dynamics study of the photodissociation of carbon monoxide from myoglobin: ligand dynamics in the first 10 ps. *Chem. Phys. 158*, 221−248.
(55) Kruglik, S. G., Lambry, J.-C., Cianetti, S., Martin, J.-L., Eady, R. R., Andrew, C. R., and Negrerie, M. (2007) Molecular basis for nitric oxide dynamics and affinity with *Alcaligenes xylosoxidans* cytochrome *c′*. *J. Biol. Chem. 282*, 5053−5062.
(56) Yoo, B.-K., Lamarre, I., Rappaport, F., Nioche, P., Raman, C. S., Martin, J.-L., and Negrerie, M. (2012) Picosecond to second dynamics reveals a structural transition in *Clostridium botulinum* NO-Sensor triggered by the activator BAY-41−2272. *ACS Chem. Biol. 7*, 2046−2054.
(57) Tani, F., Matsu-ura, M., Ariyama, K., Setoyama, T., Shimada, T., Kobayashi, S., Hayashi, T., Matsuo, T., Hisaeda, Y., and Naruta, Y. (2003) Iron twin-coronet porphyrins as models of myoglobin and hemoglobin: amphibious electrostatic effects of overhanging hydroxyl groups for successful CO/O_2 discrimination. *Chem. - Eur. J. 9*, 862−870.
(58) Laverman, L. E., and Ford, P. C. (2001) Mechanistic studies of nitric oxide reactions with water soluble iron(II), cobalt(II), and iron(III) porphyrin complexes in aqueous solutions: implications for biological activity. *J. Am. Chem. Soc. 123*, 11614−11622.

DOI: 10.1021/acschembio.6b00599
ACS Chem. Biol. 2016, 11, 3191−3201